JOURNAL OF CHEMICAL INFORMATION AND MODELING

Article

pubs.acs.org/jcim

Electronic Structure Investigation and Parametrization of Biologically Relevant Iron−Sulfur Clusters

Alexandra T. P. Carvalho[†,‡] and Marcel Swart*[,†,§]

[†]Institut de Química Computacional i Catàlisi and Departament de Química, Universitat de Girona, 17071 Girona, Spain

[‡]Department of Cell and Molecular Biology, Computational and Systems Biology, Box 596, 751 24 Uppsala, Sweden

[§]Institució Catalana de Recerca i Estudis Avançats (ICREA), Pg. Lluís Companys 23, 08010 Barcelona, Spain

Supporting Information

ABSTRACT: The application of classical molecular dynamics simulations to the study of metalloenzymes has been hampered by the lack of suitable molecular mechanics force field parameters to treat the metal centers within standard biomolecular simulation packages. These parameters cannot be generalized, nor be easily automated, and hence should be obtained for each system separately. Here we present density functional theory calculations on $[Fe_2S_2(SCH_3)_4]^{2+/+}$, $[Fe_3S_4(SCH_3)_3]^{+/0}$ and $[Fe_4S_4(SCH_3)_4]^{2+/+}$ and the derivation of parameters that are compatible with the AMBER force field. Molecular dynamics simulations performed using these parameters on respiratory Complex II of the electron transport chain showed that the reduced clusters are more stabilized by the protein environment, which leads to smaller changes in bond lengths and angles upon reduction. This effect is larger in the smaller iron−sulfur cluster, $[Fe_2S_2(SCH_3)_4]^{2+/+}$.

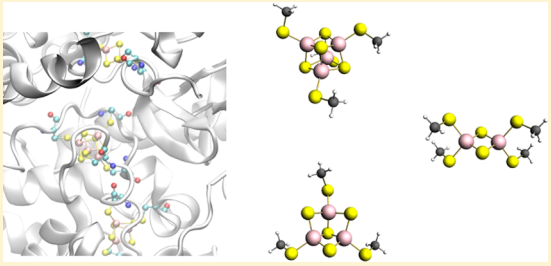

INTRODUCTION

Iron−sulfur proteins are ubiquitous in Nature, playing diverse functions such as electron transfer (ET), catalytic molecular conversions, structural roles, sensing, and regulation.[1] The most frequent activity is nevertheless biological ET. Iron−sulfur proteins are essential constituents of the mitochondrial respiratory chain, the photosynthetic ET chain and other systems of membrane bioenergetics.[1] These enzymes have reduction potentials that range from −700 to +400 mV. These finely tuned reduction potentials have evolved to facilitate ET with exceptional specificity and efficiency.[1]

There are several types of iron−sulfur clusters with different stoichiometry of the irons and sulfurs.[2−4] The most common ones are mononuclear iron coordinated by four cysteines; two irons bridged by two sulfides and coordinated by four cysteine groups, i.e., $[Fe_2S_2(SCH_3)_4]^{2+/+}$, the complete cubane $[Fe_4S_4(SCH_3)_4]^{2+/+}$ and the cubane structure with an absent iron $[Fe_3S_4(SCH_3)_4]^{+/0}$. Finally, there are the more exotic iron−sulfur clusters in the nitrogenase (N_2ase) enzyme:[5,6] $[Fe_7Mo_1S_8(SCH_3)]^q$ (FeMoco cofactor) and $[Fe_8S_7(SCH_3)_6]^q$ (the P-cluster); the former is most likely responsible for the conversion of N_2 to NH_3 and the latter for the ET processes needed for it.

These iron−sulfur clusters are complex systems, where the iron sites show large spin-polarization effects and Fe−S covalence and spin coupling; furthermore, they can display valence delocalization. Three major factors have been put forward[7−12] for the explanation of variations in the reduction potential within a single cluster type: the electrostatic environment of the redox center provided by surrounding charged amino acid residues, hydrogen bonds to the cluster, and the solvent exposure of the redox center. There exist extensive data on Fe−S experimental covalencies derived from a molecular orbital-based analysis of X-ray absorption spectroscopy (XAS) measurements, by Solomon and co-workers.[13] They found that the Fe−S covalency is significantly reduced in clusters within the protein in comparison with synthetic analogues.

A considerable amount of calculations was performed by Noodleman and co-workers on iron−sulfur cluster analogues, namely $Fe(SR)_4$, $Fe_2S_2(SR)_4$, $Fe_4S_4(SR)_4$ with R = H, CH_3. The first work reports back to 1985, where they performed $X\alpha$ valence bond scattered wave calculations on these model systems.[14] Subsequently, the same systems were studied with density functional theory (DFT) methods. The absolute reduction potentials for the Fe_2S_2 and Fe_4S_4 clusters in different oxidation states were also calculated with DFT along with a Poisson−Boltzmann treatment for the electrostatic interactions.[15−17] All these calculations have shown that the Fe−S bond is highly covalent, and that this covalency is larger for the Fe^{3+} sites than for the Fe^{2+} sites. Furthermore, the bridging sulfides were shown to be better donors than the thiolates. In the reduced states the sulfur charges become more negative because the extra electron density becomes localized mainly at the sulfurs. These calculations also suggested that in the reduced state the iron−sulfur clusters should engage in more hydrogen-bond interactions with the protein, and that

Received: December 5, 2013
Published: January 25, 2014

these hydrogen bonds would compete with sulfur-to-metal charge transfer leading to a decreased covalency. However, to unequivocally test this, larger QM models were necessary (which incorporated the protein residues that engage in the hydrogen bonds).[18,19] Yet this is not a trivial task, because a model that incorporates the entire protein or even a part containing all the hydrogen bonds to the cluster is of considerable size and hence computationally expensive. Solutions to this problem might consist of using smaller models, or performing classical molecular dynamics (MD) and trying to combine the structural information from the MD simulations with the DFT studies. However, specific force field parameters for the metals are needed to be able to perform these MD simulations.[20−24] This might in the future be circumvented by using ligand-field molecular mechanics,[25−27] but for the moment, this is not yet available with standard biomolecular simulation packages like AMBER.

The effect of hydrogen bonding on the iron−sulfur clusters has been studied also by others, e.g., by Solomon and co-workers using a synthetic Fe_4 cube that contains two hydrogen bond interactions. This $[CTA]_4[Fe_4S_4(S\text{-}t\text{Bu})_4]$ synthetic cube (CTA = carbamoyltrimethylammonium acetamide;[28] *t*Bu = *tert*-butyl) was found to be less covalent and more elongated than a normal compressed cube without hydrogen bonding present.[29] Also noteworthy are the many studies by Ichiye and co-workers on iron−sulfur complexes. These authors reported MD simulations and calculations on small models. To be able to perform the MD simulations, they developed parameters for mononuclear iron with four thiolates, $Fe(SR)_4$ (i.e., without the bridging sulfides), compatible with the CHARMM force field.[30] The bond lengths and angles were taken from a crystal structure of $Et_4N[Fe(S_2\text{-}o\text{-xyl})_2]_3$ (Et = ethane, xyl = xylyl),[31] whereas the force constants were modified to fit the CHARMM potential energy function from those of Spiro and co-workers,[32] which were based on spectroscopic data. Normal mode calculations were carried out to verify the fit to the same spectroscopic data, all of which makes these parameters highly dependent on the parameter set used at that time.[30] Early on, these authors observed[33] large differences in the surrounding protein and solvation energy in the reduced state, which were proven to be improbable in subsequent studies.[34] They started with Hartree−Fock calculations on a small monomeric iron cluster, and later on used DFT calculations on similar small systems.[35−37]

A number of DFT and nuclear magnetic resonance (NMR) studies on small $Fe(SR)_4$ models proposed a correlation between H^N-S^γ bond lengths and the variation of the reduction potential for a series of 10 rubredoxin (Rx) mutants (the H^N-S^γ bond length was observed to be shorter in the variants with higher reduction potential).[12,38] On the other hand, Sprik and co-workers calculated redox potentials using MD simulations of Rx and DFT calculations on smaller models. They showed that the hydrogen bond interactions of the cysteine ligands with the NH group of residues V8, C9, V41 and C42 are the biggest factors in the redox potential modulation, with a stronger network of hydrogen bonds leading to more positive reduction potentials.[39] Finally, Knapp and co-workers calculated[40] the redox potentials for a series of wild-type and mutant $Fe(SR)_4$ proteins and compared the reduction potential values to the experimental ones, getting a deviation of only 14 mV and showing that, for these $Fe(SR)_4$ proteins, solvent exposure plays an important role.

Here we investigated the electronic structure of three different iron−sulfur clusters that contain more than one tetrahedrally coordinated iron, and hence include the bridging sulfides. Mössbauer and electron paramagnetic resonance (EPR) studies assigned $[Fe_2S_2]^{2+}$ as $S = 0$ and $[Fe_2S_2]^{+}$ as $S = 1/2$.[41] The paramagnetic oxidized Fe_2S_2 ground state can be visualized by antiferromagnetic coupling between the two high spin ferric Fe(III) ions.[42] The $S = 1/2$ ground state for the reduced counterpart again can be explained be antiferromagnetic coupling between the high spin ferric Fe(III) and high spin ferrous Fe(II) ions. For the Fe_4S_4 cluster, which has $[Fe_4S_4]^{2+}$ $S = 0$ and $[Fe_4S_4]^{+}$ $S = 1/2$ ground-states, a similar explanation can be followed.[41,43]

The $[Fe_3S_4]^{+}$ cluster represents a particularly interesting case. A wide variety of spectroscopic techniques have been applied to these proteins, including NMR, EPR, electron nuclear double resonance (ENDOR), magnetic circular dichroism (MCD) and Mössbauer spectroscopy.[41,43] The lowest energy states are two doublets resulting from exchange coupling between the three equivalent high-spin ferric ions (Fe_i^{3+}, $S_i = 5/2$; $i = 1, 2, 3$): the two ground state doublets were proposed to be generated by exchange-coupling ferric ion 2 with ion 3 to give intermediate spin S_{23} with magnitude 2 or 3, and then coupling this spin to ion 1 to give $S_t = |S_{23} \pm S_1| = 1/2$.[41,43]

Apart from finding the ground state spin states of these clusters, we used the method of Seminario[44] to derive the force constants for the stretching and angle bending vibrations.[45] The new parameters were then used to perform molecular dynamics simulations that allowed us to quantify the number and type of hydrogen bonds between the protein and the iron−sulfur clusters. We already anticipate here that in these simulations we find that reduced clusters are more stabilized, promoted by the protein environment and leading to small variations on the bonds and angles upon reduction. This effect is larger for smaller iron−sulfur systems.

COMPUTATIONAL DETAILS

Model Systems. For our calculations, we have used the three models depicted in Figure 1. They contain, respectively, two, three and four iron atoms; two, four and four sulfide atoms; four, three and four thiolate ligands as models for the cysteine ligands, respectively. The models were based on the X-ray structure of Complex II (pdb-code 1ZOY)[46] from the oxidative phosphorylation.

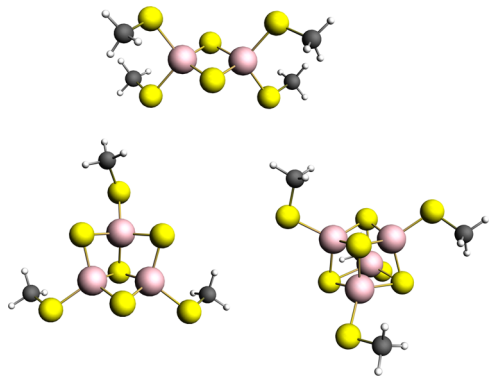

Figure 1. Structure of the different iron−sulfur clusters used in the calculations.

dx.doi.org/10.1021/ci400718m | J. Chem. Inf. Model. 2014, 54, 613−620

Table 1. $S = 5/2$ Computed Relative Energies for S Configurations (kcal·mol^{-1}) of the Oxidized and Reduced Clusters $[Fe_2S_2]^{2+}$, $[Fe_2S_2]^{+}$, $[Fe_3S_4]^{+}$, $[Fe_3S_4]^{0}$, $[Fe_4S_4]^{2+}$, $[Fe_4S_4]^{+}$

S	0	1/2	1	3/2	2	5/2	9/2	5
$[Fe_2S_2]^{2+}$	0.00	–	12.98	–	24.89			17.35
$[Fe_2S_2]^{+}$	–	0.16	–	20.09		24.02	0.00	
S	0	1/2	1	3/2	2	5/2	7	15/2
$[Fe_3S_4]^{+}$		6.26		0.00		0.05		23.15
$[Fe_3S_4]^{0}$	0.02		14.56		0.00		20.00	
S	0	1/2	1	3/2	2	5/2	17/2	9
$[Fe_4S_4]^{2+}$	0.00		11.61		19.81			37.35
$[Fe_4S_4]^{+}$		0.00		14.83		15.80	15.28	

DFT Calculations. All density functional calculations were performed with the ADF program.[47,48] Fully unrestricted calculations were performed for all the possible spin states. The lowest spin states were obtained via the broken spin symmetry approximation.

All systems were treated with the OPBE exchange-correlation functional.[49−52] Geometry optimizations and energy calculations were performed with the TZP basis set[53−55] and with the Cosmo model[56−58] with a dielectric constant of 4.0 (a lower estimate for the value found in proteins) because previously it was shown that geometry optimization in the gas phase did not give geometries with the expected accuracy when compared with experimental data.

The charges were calculated on larger models containing the entire cysteine residues. The charges employed were the multipole derived charges (MDC-d),[59] even though in AMBER force fields the common way to obtain the point charges is through gas phase HF/6-31G* calculations followed by the RESP method.[60] The main reason to adopt this procedure was that when all-atom force fields were first developed condensed phase calculations were too computationally expensive and the RESP methodology was proven to overestimate the charges making them more similar to the condensed phase ones. For consistency this method has been followed since then. However, the multipole derived charges method represents a more realistic alternative and have been successfully applied in the past to proteins.[61]

MD Simulations. MD simulations were performed with AMBER11[62] using the ff99SB parameter set[63] for the protein. An initial energy minimization was performed, followed by an equilibration of 100 ps to slowly heat the system from 0 to 300 K. The equilibration was performed in an NVT ensemble using Langevin dynamics with small restraints on the protein. Production simulations were carried out at 300 K in the NPT ensemble using Langevin dynamics with a collision frequency of 1.0 ps^{-1}. Constant pressure periodic boundary conditions were imposed with an average pressure of 1 atm. Isotropic position scaling was used to maintain pressure with a relaxation time of 2 ps. The time step was set to 2 fs. SHAKE constraints[64] were applied to all bonds involving hydrogen atoms. The particle mesh Ewald (PME) method was used to calculate electrostatic interactions with a cutoff distance of 8 Å. The total time of each of the simulations was 50 ns.

RESULTS AND DISCUSSION

DFT Calculations. The relative energies (in kcal·mol^{-1}) of the possible spin states for each cluster are shown in Table 1, with the corresponding spin-density charges given in Table 2. For the $[Fe_2S_2]^{2+/+}$ and $[Fe_4S_4]^{2+/+}$ systems our OPBE/TZP results show the expected spin ground-state, i.e., a low-spin (S = 0) for the oxidized form and a low-spin (S = 1/2) for the reduced form (see Table 1). Note that in the case of $[Fe_2S_2]^{+}$ the low-spin (S = 1/2) state is isoenergetic with the S = 9/2 state. More problematic are the $[Fe_3S_4]^{2+/+}$ systems, which when embedded within a protein show a S = 1/2 state and S = 2 state, respectively for $[Fe_3S_4]^{+}$ and $[Fe_3S_4]^{2+}$. The latter is indeed what we observe with our OPBE/TZP results (and previously by Jensen with four other density functionals).[65] However, we do not find the purported S = 1/2 state for the reduced cluster, but instead find an intermediate spin of S = 3/2, which is isoenergetic with the S = 5/2 state. This is consistent with the previous results by Jensen, where all four density functionals also gave a S = 3/2 ground-state. Our OPBE/TZP spin-state splitting between S = 1/2 and S = 3/2 is in fact quite similar to the TPSSh/6-311+G(2d,2p) result by Jensen. Given the good results in general for spin-state splittings by OPBE,[52,66−69] it is most likely that the difference between our results for the small iron−sulfur cluster and the experimentally observed spin-state for the iron−sulfur protein must be due to specific interactions between the cluster and the protein, or due to the electrostatic field of the latter. Interestingly enough, the energy of the S = 1/2 state could be obtained only by using spin-decontamination techniques[70]

Table 2. Computed Charges and Spin Densities on the Iron Atoms for the Lowest Energy Structures

$[Fe_2S_2]^{2+}$	Fe1	0.3527	2.5811		
	Fe2	0.3533	−2.5826		
		S = 9/2		S = 1/2	
$[Fe_2S_2]^{+}$	Fe1	0.4407	−2.8398	0.4011	2.4195
	Fe2	0.4401	−2.8408	0.4162	−2.6819
		S = 3/2		S = 5/2	
$[Fe_3S_4]^{+}$	Fe1	0.2369	2.4144	0.2200	2.4520
	Fe2	0.2276	−2.3895	0.3055	−2.8031
	Fe3	0.1624	−2.1035	0.3056	−2.8311
		S = 2			
$[Fe_3S_4]^{0}$	Fe1	0.2844	2.5344		
	Fe2	0.3136	−2.6600		
	Fe3	0.3090	−2.6922		
		S = 0			
$[Fe_4S_4]^{2+}$	Fe1	0.2200	2.4026		
	Fe2	0.2206	2.4263		
	Fe3	0.2184	−2.4172		
	Fe4	0.2198	−2.4240		
		S = 1/2			
$[Fe_4S_4]^{+}$	Fe1	0.2341	2.2247		
	Fe2	0.2416	2.2619		
	Fe3	0.2820	−2.5148		
	Fe4	0.2749	−2.5163		

dx.doi.org/10.1021/ci400718m | J. Chem. Inf. Model. 2014, 54, 613−620

based on the expectation values of S^2: the "$S = 1/2$" state was found to be highly contaminated and showed $\langle S^2 \rangle$-values of ca. 4.30−4.40. Not even using the spin-flip approach in ADF, nor a higher value for the dielectric constant ($\varepsilon = 30$), helped to find a "pure" $S = 1/2$ state, and the only way to get a reasonable estimate for the energy of it was by using spin-decontamination.

Molecular Mechanics Parameters. New atom types and parameters for the bond stretching and angle bending compatible with the AMBER force field were derived (see Tables 3 and S1 (Supporting Information)).

$$E = \sum_{\text{bonds}} K_r(r - r_{eq})^2 + \sum_{\text{angles}} K_\theta(\theta - \theta_{eq})^2 + \sum_{\text{torsions}} \frac{V_n}{2}(1 + \cos[n\varphi - \gamma]) + \sum_{i<j}^{\text{atoms}} \left(\frac{A_{ij}}{R_{ij}^{12}} - \frac{B}{R_{ij}^{6}} \right) + \sum_{i<j}^{\text{atoms}} \left(\frac{q_i q_j}{\varepsilon R_{ij}} \right)$$

Table 3. New Atom Types Chosen According to the Criteria of Chemical Nature, Connectivity, Location Level and Overall Geometry of the Iron−sulfur Cluster

atom types	
F2	Fe(III) in $[Fe_4S_4]^{2+}$ and $[Fe_4S_4]^{+}$
FR	Fe(II) in $[Fe_4S_4]^{+}$
S1	sulfur of the cysteinyl groups
S2	S^{2-} connected to two iron atoms
S3	S^{2-} connected to three iron atoms
FA	Fe(III) in $[Fe_3S_4]^{+}$ and in $[Fe_3S_4]^{0}$
FB	Fe(III) in $[Fe_3S_4]^{+}$
FC	Fe(II) in $[Fe_3S_4]^{0}$
FD	Fe in $[Fe_4S_4]^{2+}$
FU	Fe in $[Fe_4S_4]^{2+}$
SD	sulfur connected to three irons in $[Fe_4S_4]^{2+}$
SU	sulfur connected to three irons in $[Fe_4S_4]^{2+}$
FY	Fe in $[Fe_4S_4]^{+}$
F4	Fe in $[Fe_4S_4]^{+}$

The definition of an atom type is mainly based on three criteria: chemical nature, bond connectivity and location level (side chain or backbone), and we also included, as criterion, the geometry of the iron−sulfur clusters. According to these considerations, we have used the minimum number of new atom types to describe our systems (see Table 3).

Parameter Validations. We have gone through a detailed structural comparison among MD structures, DFT optimized structures and the X-ray structure (PDB code: 1ZOY).[46] We have to stress that our procedure corroborates the high accuracy in bonds and angles values obtained from the DFT calculations with COSMO ($\varepsilon = 4$) with a physical description of the environment (remaining protein and explicit solvent). Using this procedure, we have found that the average bond lengths, angles and dihedrals are similar to the QM and X-ray structures and that they fluctuate very little during the course of the simulations (Tables S2A−C, Supporting Information). The reduced clusters have slightly larger Fe−S bond distances than the oxidized ones both in the DFT optimized small models and in the simulations. This has been observed before for other iron−sulfur clusters and has been attributed to a greater antibonding character in the reduced state by the unpaired electrons. The fact that the obtained force constants allow to correctly represent slight changes in bond distances further shows how a simple molecular mechanics method, as long as it is correctly parametrized,[71] allows to correctly reproduce the QM derived geometric properties.

The $[Fe_4S_4]^{2+}$ Fe−S_{Cys} DFT bond distance is 2.28 Å and the simulation average is 2.28 ± 0.06 Å. In the reduced $[Fe_4S_4]^{+}$ cluster, the bond distances are 2.31 Å in the DFT model and 2.30 ± 0.06 Å in the simulation. For the oxidized $[Fe_3S_4]^{+}$ cluster, the Fe−S_{Cys} bond distance in the DFT model is 2.25 Å and in the simulation it is 2.25 ± 0.06 Å, whereas for reduced $[Fe_3S_4]^{0}$, the Fe−S_{Cys} bond distance from DFT is 2.35 Å and in the simulation it is 2.34 ± 0.07 Å.

MD Simulations. It has long been recognized that the protein environment modulates the properties of Fe−S bonds to achieve the desired function and stability.[72] In mononuclear iron−sulfur complexes, it was proposed that the amide groups of the protein backbone finely tune the reduction potentials, that is, redox potentials are shifted positively by the presence of N−H···S hydrogen bonds. In fact, in the case of rubredoxin (Rx), Sulpizi and co-workers found that a small QM model with hydrogen bonds only to Val8, Cys9, Leu41 and Cys42 was able to modulate the redox potential of Rx.[39] Similarly, Lin and co-workers found that the mutation of Val44 to Ile, Ala or Gly shortens the N−H···S Hydrogen bond (which correlates with the increase in reduction potential).[12] More recently, it was shown that an increase of the N−H···S^{γ} bond strength leads to a decrease in the mechanical stability of Fe(III)−thiolate bonds, and therefore the differences in reduction potential can be a direct consequence of the modulation of the Fe−S bond strength.[73] The reasoning for these trends was that the formation of hydrogen bonds influences the electron delocalization between sulfur and iron, in turn leading to a decreased covalency.

In our MD simulations, we observe that the reduced clusters establish more and stronger interactions with the surrounding protein environment (see Table 4). The additional and shorter hydrogen bonds should allow for more efficient delocalization (and stabilization) of the negative charge in the reduced state. Hence, in small iron−sulfur systems such as the small models we have considered for this study, which are not stabilized by the protein amide groups, the charge is more concentrated at the sulfur atoms. The amide groups establish hydrogen bonds with the sulfur atoms which leads to electron delocalization, and then to weaker Fe(III)−S bonds. However, with Fe(II) we have one additional electron in the system, and hence the amide groups stabilize the extra negative charge of the sulfurs. The systems are more similar between the oxidized and reduced states, requiring less inner reorganization energy from going from one state to the other and as such the electron transfer reactions are faster and more efficient.

In our simulations, the only large structural discrepancy we found (compared to experimental data) was for the reduced $[Fe_2S_2]^{+}$ cluster because, in this case, the Fe(III)−S_{Cys} and Fe(II)−S_{Cys} average bond distances from the simulation (see Table S2A, Supporting Information) are significantly smaller than those in the QM small model. The F2−S1 distance is 2.22 ± 0.09 Å in the simulation compared to 2.34 Å in the small QM model, whereas the FR−S1 is 2.29 ± 0.08 Å in the simulation and 2.38 Å in the QM model. In a similar way the F2−S2 bond distances are 2.18 ± 0.06 Å and 2.24 ± 0.06 Å in the simulation and 2.21 Å and 2.29 Å in the QM model (see Table S2A, Supporting Information).

dx.doi.org/10.1021/ci400718m | J. Chem. Inf. Model. 2014, 54, 613−620

Table 4. Hydrogen Bonds Formed between the Sulfur Atoms and the Protein Environment

		$[Fe_2S_2]^{2+}$	
		distance	angle
Cys-B65 NH	Cys-B70 S1	2.8 ± 0.24	155.9 ± 12.5
Ile-B69	Cys-B65 S1	2.44 ± 0.19	156.4 ± 10
		$[Fe_2S_2]^{+}$	
		distance	angle
Cys-B65 NH	Cys-B70 S1	2.52 ± 0.21	165.7 ± 8.5
Cys-B70 NH	Cys-B65 S1	2.53 ± 0.25	138.0 ± 15.3
Cys-B73 NH	S2	2.60 ± 0.24	163.4 ± 9.4
Arg-B66 NH	S1	2.21 ± 0.16	149.1 ± 12.7
Ile-B69 NH	S2	2.37 ± 0.16	159.1 ± 12.7
		$[Fe_4S_4]^{2+}$	
		distance	angle
Cys-B163 NH	Cys-B161 S	2.96 ± 0.32	139.1 ± 12.9
Leu-B160 NH	Cys-B158 S	2.45 ± 0.18	156.6 ± 8.1
Ala-B162 NH	S1	2.50 ± 0.22	159.5 ± 8.0
Ile-B159 NH	S4	2.66 ± 0.24	157.0 ± 7.5
		$[Fe_4S_4]^{+}$	
		distance	angle
Cys-B163 NH	Cys-B161 S	2.71 ± 0.29	158.9 ± 7.9
Leu-B160 NH	Cys-B158 S	2.39 ± 0.18	154.4 ± 7.8
Cys-B164 NH	S3	2.63 ± 0.26	140.4 ± 12.5
Ala-B162 NH	S1	2.41 ± 0.19	140.4 ± 12.4
		$[Fe_3S_4]^{+}$	
		distance	angle
His-B216 NH	S1	2.34 ± 0.24	145.9 ± 17.5
Met-B219 NH	S2	2.34 ± 0.18	149.2 ± 9.9
Thr-B217 NH	Cys-B215 S	2.52 ± 0.21	152.4 ± 8.6
Tyr-B178 OH	S3	2.37 ± 0.21	148.9 ± 14.4
		$[Fe_3S_4]^{0}$	
		distance	angle
His-B216 NH	S1	2.52 ± 0.33	138.8 ± 18.1
Met-B219 NH	S2	2.31 ± 0.18	151.3 ± 9.1
Asn-B215 NH	S4	2.50 ± 0.23	138 ± 14.14
Thr-B217 NH	Cys-B215 S	2.47 ± 0.20	147.3 ± 8.5
Tyr-B178 OH	S3	2.29 ± 0.19	149.3 ± 13.2
Ser-B170 OH	S1	2.54 ± 1.10	154.4 ± 23.2

Due to this difference between the small QM model and the simulation, we constructed a 185-atom QM model of this system (Figure 2). This model contains all direct (covalent, hydrogen bonding) interactions to the sulfur atoms. In this case, the Fe−S distances are 2.31, 2.33, 2.24 and 2.27 Å, respectively, much more similar to the structures from the MD simulation (see Table S2A, Supporting Information). Therefore, the inclusion of part of the protein results in smaller values for the Fe−S bond distances. This effect occurs because the charge located at the sulfur atoms is smaller, because the sulfurs are now more stabilized by the amide groups. Hence, the major problem with our force field description was that the point charges calculated from a small model are overestimated, leading to small distances for this system. However, even with all these limitations the values we obtained for the deviations in $[Fe_2S_2(SR)_4]^{2+/+}$ bonds and angles in the simulations are very reasonable. A more accurate solution could be using larger systems for determination of the charges, but then we would have to define a large number of residues different from the ones of the standard force field to account for changes in the

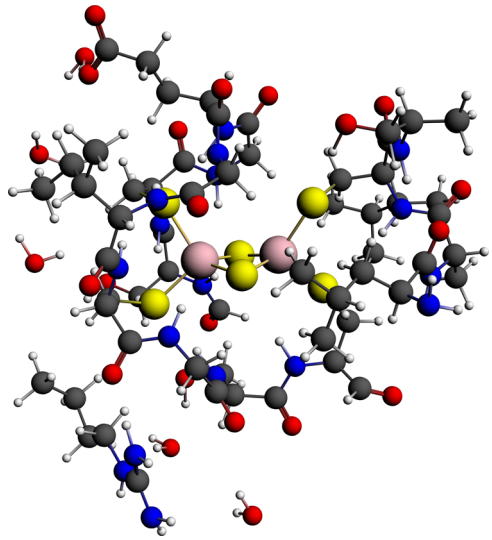

Figure 2. Larger model including all the residues interacting directly with the cluster.

point charges. After all, we are adding parameters to an existing force field, so the inclusion of different residues with different point charges in the backbone must be tested. In fact, we are carrying out this study for a smaller mononuclear iron−sulfur system to check the validity of this approximation. We can even wonder if a polarizable description of the protein environment would be more adequate for the $[Fe_2S_2]^{+}$ reduced system, which is something we want to address in future studies. It is interesting to point out that this effect is much higher for the $[Fe_2S_2]^{+}$ iron−sulfur cluster than for the reduced $[Fe_3S_4]^{0}$ and $[Fe_4S_4]^{+}$ clusters. These latter clusters seem to depend less on the protein environment. The larger number of iron and sulfur atoms could make that the extra electron, after reduction, be more easily introduced into the system with minimum variation in geometric parameters.

Another thing to point out is that these iron−sulfur clusters are considerably more buried in the protein than the mononuclear iron−sulfur clusters in small proteins such as rubredoxin or desulforedoxin, which are largely solvent exposed.[40] Nevertheless, in Complex II there is a chain of water molecules between the two protein active sites that has been linked to the proton uptake pathway. However, we have not found any waters directly interacting with the iron−sulfur clusters, except in the case of $[Fe_3S_4]^{+/0}$, where one of the inorganic sulfurs interacts with a water molecule. The average number of water molecules at 3.5 Å from the S2 atom is 0.87 ± 0.34 for the oxidized cluster and 0.97 ± 0.19 for the reduced one.

Our derived bond parameters can be applied to other systems. However, special care must be taken for the calculation of charges. There are no similar parameters in the literature for these types of systems for the AMBER force field. There are, however, other studies using MD simulations that were made with constraints or arbitrary force constants, such as the study of HiPIP from *Chromatium vinosum*.[30] In this example from the literature, the simulations were made by constraining the bond lengths with SHAKE to the starting X-ray values, and hence no force constants were used for the bond stretching. For the bending constants, it was found that the values derived from the analysis of vibrational spectra were too low to maintain the geometry of the clusters; to maintain the geometries during the

dx.doi.org/10.1021/ci400718m | J. Chem. Inf. Model. 2014, 54, 613−620

simulations the force constant values had to be scaled.[30] On the contrary, we have derived all the parameters for bond stretching and angle bending directly from the second derivative matrix of a QM optimized structure. Therefore, our parameters allowed a correct representation of the clusters with no necessity of scaling.

CONCLUSIONS

We have conducted electronic structure calculations on three iron−sulfur clusters that are very important from a biological point of view. We have tested all possible spin states, resorting to broken symmetry DFT calculations with the OPBE exchange-correlation functional.

From the ground state structure Hessian matrices, we extracted force constants for the bonds and angles for which we used Seminario's method. We also calculated new charges. These parameters were employed to performed classical molecular dynamics simulations on the complex II or SQR within a lipid membrane and with an explicit solvent description.

We observed that in the small DFT models (even with a continuum solvent description with dielectric constant of 4) the bonds and angles for the reduced clusters are slightly overestimated compared to the X-ray values. In the simulations, these values are smaller and more similar to experimental data. This is quite evident in the case of the reduced $[Fe_2S_2]^+$ cluster. In this case, in the smaller model system, the bonds are overestimated, whereas in a larger DFT model containing all the residues that interact directly with the cluster (including a continuum model for the protein environment and solvent), the bonds have smaller values, which are much more similar to the values obtained in the simulations or the X-ray values.

Consequently, the protein environment seems to stabilize the reduced clusters, making the Fe−S bonds shorter. One explanation for the stabilization of the reduced clusters we observed is the fact that they establish more and shorter hydrogen bonds with the protein amide groups. However we cannot rule out other factors such as solvent exposure or charged residues in the vicinity, since in the simulations all of these factors are taken in account. The correct separation of all of these different interactions is not a trivial task, but our new force field parameters open the way to new studies and to further progress in the field.

ASSOCIATED CONTENT

Supporting Information

Bond stretching force constants, equilibrium distances, and comparison of the bonds and angles for $[Fe_2S_2]^{2+/+}$, $[Fe_4S_4]^{2+/+}$ and $[Fe_3S_4]^{+/0}$. This material is available free of charge via the Internet at http://pubs.acs.org.

AUTHOR INFORMATION

Corresponding Author

*M. Swart.

Notes

The authors declare no competing financial interest.

ACKNOWLEDGMENTS

The following organizations are thanked for financial support: The AGAUR for the fellowship 2010 BP_B00238, the Ministerio de Ciencia e Innovación (MICINN, project number CTQ2011-25086/BQU) and the DIUE of the Generalitat de Catalunya (project number 2009SGR528, and Xarxa de Referència en Química Teòrica i Computacional). Financial support from MICINN (Ministry of Science and Innovation, Spain) and the FEDER fund (European Fund for Regional Development) was provided by grant UNGI08-4E-003. With the support of the Secretary for Universities and Research of the Ministry of Economy and Knowledge of the Government of Catalonia and the Cofund programme of the Marie Curie Actions of the seventh R&D Framework Programme of the European Union. The authors are also grateful to the computer resources, technical expertise, and assistance provided by the Barcelona Supercomputing Center—Centro Nacional de Supercomputación.

REFERENCES

(1) Beinert, H.; Holm, R. H.; Münck, E. Iron-sulfur clusters: nature's modular, multipurpose structures. *Science* **1997**, *277* (5326), 653−9.

(2) Fraústo do Silva, J. J. R.; Williams, R. J. P., *The Biological Chemistry of the Elements. The Inorganic Chemistry of Life*, Paperback ed.; Oxford University Press: Oxford, U.K., 1991.

(3) Lippard, S. J.; Berg, J. M. *Principles of bioinorganic chemistry*; University Science Books: Mill Valley, CA, 1994.

(4) Bertini, I.; Gray, H. B.; Stiefel, E. I.; Valentine, J. S. *Biological Inorganic Chemistry: Structure and Reactivity*; University Science: Sausalito, CA, 2007.

(5) Einsle, O.; Tezcan, F. A.; Andrade, S. L. A.; Schmid, B.; Yoshida, M.; Howard, J. B.; Rees, D. C. Nitrogenase MoFe-Protein at 1.16 Å Resolution: A Central Ligand in the FeMo-Cofactor. *Science* **2002**, *297*, 1696−1700.

(6) Lancaster, K. M.; Roemelt, M.; Ettenhuber, P.; Hu, Y.; Ribbe, M. W.; Neese, F.; Bergmann, U.; DeBeer, S. X-ray Emission Spectroscopy Evidences a Central Carbon in the Nitrogenase Iron-Molybdenum Cofactor. *Science* **2011**, *334*, 974−977.

(7) Kassner, R. J. Effects of nonpolar environments on the redox potentials of heme complexes. *Proc. Natl. Acad. Sci. U. S. A.* **1972**, *69* (8), 2263−7.

(8) Adman, E.; Watenpaugh, K. D.; Jensen, L. H. NH—S hydrogen bonds in Peptococcus aerogenes ferredoxin, Clostridium pasteurianum rubredoxin, and Chromatium high potential iron protein. *Proc. Natl. Acad. Sci. U. S. A.* **1975**, *72* (12), 4854−8.

(9) Carter, C. W. New stereochemical analogies between iron-sulfur electron transport proteins. *J. Biol. Chem.* **1977**, *252* (21), 7802−7811.

(10) Rodgers, K. K.; Sligar, S. G. Surface electrostatics, reduction potentials, and the internal dielectric constant of proteins. *J. Am. Chem. Soc.* **1991**, *113* (24), 9419−9421.

(11) Bertrand, P.; Mbarki, O.; Asso, M.; Blanchard, L.; Guerlesquin, F.; Tegoni, M. Control of the redox potential in c-type cytochromes: importance of the entropic contribution. *Biochemistry* **1995**, *34* (35), 11071−9.

(12) Lin, I. J.; Gebel, E. B.; Machonkin, T. E.; Westler, W. M.; Markley, J. L. Changes in hydrogen-bond strengths explain reduction potentials in 10 rubredoxin variants. *Proc. Natl. Acad. Sci. U. S. A.* **2005**, *102* (41), 14581−6.

(13) Rose, K.; Shadle, S. E.; Eidsness, M. K.; Kurtz, D. M.; Scott, R. A.; Hedman, B.; Hodgson, K. O.; Solomon, E. I. Investigation of iron-sulfur covalency in rubredoxins and a model system using sulfur K-edge X-ray absorption spectroscopy. *J. Am. Chem. Soc.* **1998**, *120* (41), 10743−10747.

(14) Noodleman, L.; Norman, J. G.; Osborne, J. H.; Aizman, A.; Case, D. A. Models for Ferredoxins - Electronic-Structures of Iron Sulfur Clusters with One, 2, and 4 Iron Atoms. *J. Am. Chem. Soc.* **1985**, *107* (12), 3418−3426.

(15) Mouesca, J. M.; Chen, J. L.; Noodleman, L.; Bashford, D.; Case, D. A. Density-Functional Poisson-Boltzmann Calculations of Redox Potentials for Iron-Sulfur Clusters. *J. Am. Chem. Soc.* **1994**, *116* (26), 11898−11914.

(16) Noodleman, L.; Li, J.; Fisher, C. L.; Nelson, M. R.; Bashford, D.; Case, D. A.; Hendrickson, D. N.; Adams, D. M. Electronic structure calculations: Density functional calculations of spin polarization, spin and charge transfer, and solvent/environmental effects in transition metal complexes. *Abstr. Pap. Am. Chem. Soc.* **1997**, *213*, 71−INOR.
(17) Torres, R. A.; Lovell, T.; Noodleman, L.; Case, D. A. Density functional-and reduction potential calculations of Fe(4)S(4) clusters. *J. Am. Chem. Soc.* **2003**, *125* (7), 1923−1936.
(18) Noodleman, L.; Peng, C. Y.; Mouusca, J. M.; Case, D. A. Orbital Interactions, Electron Delocalization, and Spin Coupling in Iron-Sulfur Clusters - a Density-Functional Perspective. *Abstr. Pap. Am. Chem. Soc* **1995**, *209*, 152−COMP.
(19) Noodleman, L.; Peng, C. Y.; Case, D. A.; Mouesca, J. M. Orbital Interactions, Electron Delocalization and Spin Coupling in Iron-Sulfur Clusters. *Coord. Chem. Rev.* **1995**, *144*, 199−244.
(20) Hu, L.; Ryde, U. Comparison of Methods to Obtain Force-Field Parameters for Metal Sites. *J. Chem. Theory Comput.* **2011**, *7*, 2452−2463.
(21) Norrby, P.-O.; Brandt, P. Deriving force field parameters for coordination complexes. *Coord. Chem. Rev.* **2001**, *212*, 79−109.
(22) Zimmer, M. Are classical molecular mechanics calculations still useful in bioinorganic simulations? *Coord. Chem. Rev.* **2009**, *253*, 817−826.
(23) Banci, L. Molecular dynamics simulations of metalloproteins. *Curr. Opin. Chem. Biol.* **2003**, *7*, 143−149.
(24) Deeth, R. J. General Molecular Mechanics Method for Transition Metal Carboxylates and its Application to the Multiple Coordination Modes in Mono- and Dinuclear Mn(II) Complexes. *Inorg. Chem.* **2008**, *47*, 6711−6725.
(25) Handley, C. M.; Deeth, R. J.; Multi-Objective, A. Approach to Force Field Optimization: Structures and Spin State Energetics of d6 Fe(II) Complexes. *J. Chem. Theory Comput.* **2012**, *8*, 194−202.
(26) Deeth, R. J. The ligand field molecular mechanics model and the stereoelectronic effects of d and s electrons. *Coord. Chem. Rev.* **2001**, *212*, 11−34.
(27) Deeth, R. J.; Anastasi, A.; Diedrich, C.; Randell, K. Molecular modelling for transition metal complexes: Dealing with d-electron effects. *Coord. Chem. Rev.* **2009**, *253*, 795−816.
(28) Walters, M. A.; Roche, C. L.; Rheingold, A. L.; Kassel, S. W. N-H···S Hydrogen Bonds in a Ferredoxin Model. *Inorg. Chem.* **2005**, *44* (11), 3777−3779.
(29) Dey, A.; Roche, C. L.; Walters, M. A.; Hodgson, K. O.; Hedman, B.; Solomon, E. I. Sulfur K-edge XAS and DFT calculations on [Fe4S4](2+) clusters: Effects of H-bonding and structural distortion on covalency and spin topology. *Inorg. Chem.* **2005**, *44* (23), 8349−8354.
(30) Shenoy, V. S.; Ichiye, T. Influence of Protein Flexibility on the Redox Potential of Rubredoxin - Energy Minimization Studies. *Proteins* **1993**, *17* (2), 152−160.
(31) Lane, R. W.; Ibers, J. A.; Frankel, R. B.; Holm, R. H. Synthetic analogs of active sites of iron-sulfur proteins: bis (o-xylyldithiolato) ferrate (III) monoanion, a structurally unconstrained model for the rubredoxin Fe-S4 unit. *Proc. Natl. Acad. Sci. U. S. A.* **1975**, *72*, 2868−2872.
(32) Spiro, T. G. *Iron-Sulfur Proteins*; Wiley: New York, 1982.
(33) Yelle, R. B.; Park, N. S.; Ichiye, T. Molecular-Dynamics Simulations of Rubredoxin from Clostridium Pasteurianum - Changes in Structure and Electrostatic Potential during Redox Reactions. *Proteins* **1995**, *22* (2), 154−167.
(34) Ergenekan, C. E.; Thomas, D.; Fischer, J. T.; Tan, M. L.; Eidsness, M. K.; Kang, C. H.; Ichiye, T. Prediction of reduction potential changes in rubredoxin: A molecular mechanics approach. *Biophys. J.* **2003**, *85* (5), 2818−2829.
(35) Swartz, P. D.; Beck, B. W.; Ichiye, T. Structural origins of redox potentials in Fe-S proteins: Electrostatic potentials of crystal structures. *Biophys. J* **1996**, *71* (6), 2958−2969.
(36) Luo, Y.; Niu, S. Q.; Ichiye, T. Understanding Rubredoxin Redox Sites by Density Functional Theory Studies of Analogues. *J. Phys. Chem. A* **2012**, *116* (35), 8918−8924.
(37) Niu, S. Q.; Nichols, J. A.; Ichiye, T. Optimization of Spin-Unrestricted Density Functional Theory for Redox Properties of Rubredoxin Redox Site Analogues. *J. Chem. Theory Comput.* **2009**, *5* (5), 1361−1368.
(38) Wilkens, S. J.; Xia, B.; Weinhold, F.; Markley, J. L.; Westler, W. M. NMR investigations of Clostridium pasteurianum rubredoxin. Origin of hyperfine H-1, H-2, C-13 and N-15 NMR chemical shifts in iron-sulfur proteins as determined by comparison of experimental data with hybrid density functional calculations. *J. Am. Chem. Soc.* **1998**, *120* (19), 4806−4814.
(39) Sulpizi, M.; Raugei, S.; VandeVondele, J.; Carloni, P.; Sprik, M. Calculation of Redox Properties: Understanding Short- and Long-Range Effects in Rubredoxin. *J. Phys. Chem. B* **2007**, *111* (15), 3969−3976.
(40) Gamiz-Hernandez, A. P.; Kieseritzky, G.; Ishikita, H.; Knapp, E. W. Rubredoxin Function: Redox Behavior from Electrostatics. *J. Chem. Theory Comput.* **2011**, *7*, 742−752.
(41) Cammack, R.; Berliner, L. Electron Magnetic Resonance of Iron−Sulfur Proteins in Electron-Transfer Chains: Resolving Complexity. In *Metals in Biology: Applications of High-Resolution EPR to Metalloenzymes*; Graeme, H., Berliner, L., Eds; Springer: New York, 2010; Vol. *29*.
(42) Schreiner, E.; Nair, N. N.; Pollet, R.; Staemmler, V.; Marx, D. Dynamical magnetostructural properties of Anabaena ferredoxin. *Proc. Natl. Acad. Sci. U. S. A.* **2007**, *104* (52), 20725−30.
(43) Banci, L.; Bertini, I.; Luchinat, C.; Turano, P. Special cofactors and metal clusters. In *Biological Inorganic Chemistry: Structure and Reactivity*, Bertini, I., Ed.; University Science Books: Mill Valley, CA, **2007**.
(44) Seminario, J. M. Calculation of Intramolecular Force fields from second-derivative tensors. *Int. J. Quantum Chem., Quantum Chem. Symp.* **1996**, *30*, 59−65.
(45) Reyes, L. H.; Seminario, J. M. Determination of precise harmonic force constants for alanine polypeptides. *J. Mol. Struct.: THEOCHEM* **2007**, *818* (1−3), 125−129.
(46) Sun, F.; Huo, X.; Zhai, Y.; Wang, A.; Xu, J.; Su, D.; Bartlam, M.; Rao, Z. Crystal structure of mitochondrial respiratory membrane protein complex II. *Cell* **2005**, *121* (7), 1043−57.
(47) te Velde, G.; Bickelhaupt, F. M.; Baerends, E. J.; Fonseca Guerra, C.; van Gisbergen, S. J. A.; Snijders, J. G.; Ziegler, T. Chemistry with ADF. *J. Comput. Chem.* **2001**, *22* (9), 931−967.
(48) Fonseca Guerra, C.; Snijders, J. G.; te Velde, G.; Baerends, E. J. Towards an order-N DFT method. *Theor. Chem. Acc.* **1998**, *99* (6), 391−403.
(49) Handy, N. C.; Cohen, A. J. Left-right correlation energy. *Mol. Phys.* **2001**, *99* (5), 403−412.
(50) Perdew, J. P.; Burke, K.; Ernzerhof, M. Generalized Gradient Approximation Made Simple. *Phys. Rev. Lett.* **1996**, *77* (18), 3865−3868.
(51) Swart, M.; Ehlers, A. W.; Lammertsma, K. Performance of the OPBE exchange-correlation functional. *Mol. Phys.* **2004**, *102* (23−24), 2467−2474.
(52) Swart, M. Accurate Spin-State Energies for Iron Complexes. *J. Chem. Theory Comput.* **2008**, *4* (12), 2057−2066.
(53) Van Lenthe, E.; Baerends, E. J. Optimized Slater-type basis sets for the elements 1−118. *J. Comput. Chem.* **2003**, *24* (9), 1142−1156.
(54) Chong, D. P.; Van Lenthe, E.; Van Gisbergen, S.; Baerends, E. J. Even-tempered slater-type orbitals revisited: From hydrogen to krypton. *J. Comput. Chem.* **2004**, *25* (8), 1030−1036.
(55) Chong, D. P. Augmenting basis set for time-dependent density functional theory calculation of excitation energies: Slater-type orbitals for hydrogen to krypton. *Mol. Phys.* **2005**, *103* (6−8), 749−761.
(56) Klamt, A.; Schuurmann, G. COSMO: a new approach to dielectric screening in solvents with explicit expressions for the screening energy and its gradient. *J. Chem. Soc., Perkin Trans. 2* **1993**, *0* (5), 799−805.
(57) Pye, C. C.; Ziegler, T. An implementation of the conductor-like screening model of solvation within the ADF package. *Theor. Chem. Acc.* **1999**, *101*, 396−408.

(58) Swart, M.; Rösler, E.; Bickelhaupt, F. M. Proton affinities in water of maingroup-element Hydrides - Effects of hydration and methyl substitution. *Eur. J. Inorg. Chem.* **2007**, *23*, 3646−3654.
(59) Swart, M.; van Duijnen, P. T.; Snijders, J. G. A charge analysis derived from an atomic multipole expansion. *J. Comput. Chem.* **2001**, *22* (1), 79−88.
(60) Bayly, C. I.; Cieplak, P.; Cornell, W.; Kollman, P. A. A well-behaved electrostatic potential based method using charge restraints for deriving atomic charges: the RESP model. *J. Phys. Chem.* **1993**, *97* (40), 10269−10280.
(61) Groenhof, A. R.; Ehlers, A. W.; Lammertsma, K. Proton assisted oxygen-oxygen bond splitting in cytochrome p450. *J. Am. Chem. Soc.* **2007**, *129* (19), 6204−9.
(62) Case, D. A.; Darden, T. A.; Cheatham, I. T. E.; Simmerling, C. L.; Wang, J.; Duke, R. E.; Luo, R.; Crowley, M.; Walker, R. C.; Zhang, W.; Merz, K. M.; Wang, B., AMBER 10. University of California, San Francisco: San Francisco, CA, 2008.
(63) Hornak, V.; Abel, R.; Okur, A.; Strockbine, B.; Roitberg, A.; Simmerling, C. Comparison of multiple Amber force fields and development of improved protein backbone parameters. *Proteins* **2006**, *65* (3), 712−25.
(64) Ryckaert, J.-P.; Ciccotti, G.; Berendsen, H. J. C. Numerical integration of the cartesian equations of motion of a system with constraints: molecular dynamics of n-alkanes. *J. Comput. Phys.* **1977**, *23* (3), 327−341.
(65) Jensen, K. P. Computational studies of modified [Fe3S4] clusters: why iron is optimal. *J. Inorg. Biochem.* **2008**, *102* (1), 87−100.
(66) Swart, M.; Groenhof, A. R.; Ehlers, A. W.; Lammertsma, K. Validation of Exchange−Correlation Functionals for Spin States of Iron Complexes. *J. Phys. Chem. A* **2004**, *108* (25), 5479−5483.
(67) Jensen, K. P. Bioinorganic Chemistry Modeled with the TPSSh Density Functional. *Inorg. Chem.* **2008**, *47* (22), 10357−10365.
(68) Jensen, K. P.; Cirera, J. Accurate Computed Enthalpies of Spin Crossover in Iron and Cobalt Complexes. *J. Phys. Chem. A* **2009**, *113* (37), 10033−10039.
(69) Zlatar, M.; Gruden-Pavlovic, M.; Guell, M.; Swart, M. Computational study of the spin-state energies and UV-Vis spectra of bis(1,4,7-triazacyclononane) complexes of some first-row transition metal cations. *Phys. Chem. Chem. Phys.* **2013**, *15*, 6631−6639.
(70) Swart, M.; Güell, M.; Luis, J. M.; Solà, M. Spin-State-Corrected Gaussian-Type Orbital Basis Sets. *J. Phys. Chem. A* **2010**, *114* (26), 7191−7197.
(71) Carvalho, A. T. P. Biomolecular Simulations of Metalloenzymes: Strategies to Tackle the Missing Parameter Problem. *Curr. Inorg. Chem.* **2012**, *2* (3), 254−262.
(72) Capozzi, F.; Ciurli, S.; Luchinat, C. Coordination sphere versus protein environment as determinants of electronic and functional properties of iron-sulfur proteins. In *Metal Sites in Proteins and Models Redox Centres*; Hill, H. A. O., Sadler, P. J., Thomson, A. J., Eds.; Springer: Berlin, Heidelberg, 1998; Vol. *90*, pp 127−160.
(73) Zheng, P.; Takayama, S. J.; Mauk, A. G.; Li, H. Hydrogen bond strength modulates the mechanical strength of ferric-thiolate bonds in rubredoxin. *J. Am. Chem. Soc.* **2012**, *134* (9), 4124−31.